STRUCTURE AND OPTICAL PROPERTIES OF Eu^{3+}-DOPED AL_2O_3 NANOPARTICLES SYNTHESIZED BY COPRECIPITATION METHOD

Đến tòa soạn 15-05-2024

Bui Hong Van[1], Nguyen Thi Dao[1], Tran Kim Anh[2], Pham Minh Chau[2], Nguyen Duc Ba[2], Nguyen Tien Dai[2,3], Dang Van Thai[2,4*]

1. VNU University of Science, Vietnam National University - Hanoi, Vietnam

2. Institute of Theoretical and Applied Research, Duy Tan University, Hanoi 100000, Vietnam

3. Faculty of Natural Sciences, Duy Tan University, Da Nang 550000, Vietnam

4. Faculty of Environmental and Chemical Engineering, Duy Tan University, Da Nang 550000, Vietnam

*Email: dangvanthai2@duytan.edu.vn

TÓM TẮT

CẤU TRÚC VÀ CÁC ĐẶC TÍNH QUANG CỦA CÁC HẠT NANO AL_2O_3 PHA TẠP Eu^{3+} TỔNG HỢP BẰNG PHƯƠNG PHÁP ĐỒNG KẾT TỦA

Các hạt nano (NPs) Al_2O_3 pha tạp ion Eu^{3+} (Al_2O_3:Eu^{3+}) được chế tạo bằng phương pháp đồng kết tủa. Pha cấu trúc hỗn hợp α- Al_2O_3 và γ- Al_2O_3 của tinh thể được hình thành ở nhiệt độ ủ 400 ^0C trong thời gian ủ 2 h. Kích thước hạt tinh thể trung bình khoảng 12 - 15 nm. Độ rộng vùng cấm (E_g) của Al_2O_3 giảm từ 5.26 đến 4.72 eV do sự thay thế ion Eu^{3+}. Phổ phát quang (PL) của Al_2O_3:Eu^{3+} với cực đại ở 614 nm đặc trưng cho chuyển dời $^5D_0 \rightarrow {}^7F_2$ của các ion Eu^{3+}. Tỉ số bất đối xứng (R_{21}) giữa cường độ vạch $^5D_0 \rightarrow {}^7F_2$ và $^5D_0 \rightarrow {}^7F_1$ bằng 3.02 cho biết độ bất đối xứng cao của môi trường xung quanh các ion Eu^{3+} trong tinh thể. Đặc tính PL mạnh ở 614 nm của Al_2O_3:Eu^{3+} có tiềm năng cho các ứng dụng quang điện tử và y sinh.

Từ khóa: *vật liệu α- Al_2O_3 và γ- Al_2O_3, hạt nano Al_2O_3:Eu^{3+}, Al_2O_3 pha tạp Eu^{3+}, phát xạ ion Eu^{3+}, phát quang.*

1. Introduction

Al_2O_3:Eu^{3+} nanomaterial is widely applied for optoelectronics [1], fingerprint identification [2], and transparent ceramics [3]. The Al_2O_3:Eu^{3+} can be synthesized by many different methods, such as hydrothermal method [4], sol-gel [5], combustion [6], slipcasting [3], and coprecipitation [7]. However, the Eu^{3+} radius (0.95 Å) is larger than the Al^{3+} radius (0.54 Å) [6], so the Eu^{3+} ion replacement into the Al_2O_3 host lattice is not easy, requiring a suitable manufacturing process. The crystal structure phase can exist in different forms of α, β, γ, θ, and η, depending on the annealing temperature. At low annealing temperatures, the α and γ phases are major [1]. At high annealing temperatures, the structure phase changes to the α form [8]. The band gap energy (E_g) of Al_2O_3 ranges widely from 5.1 to 9.4 eV, depending on the crystal structure

phase [1, 9, 10]. The photoluminescence (PL) spectrum shows a broad band in the 350 – 500 nm range caused by defects [5]. When Eu^{3+} ions are incorporated into the Al_2O_3 crystal lattice, the PL spectrum of $Al_2O_3:Eu^{3+}$ nanoparticles (NPs) consists of two bands. The PL band of defects has a fragile intensity and almost disappears completely [11]. The PL band of Eu^{3+} ions has a vigorous intensity, originating from six transitions $^5D_0 - {}^7F_J$ (J = 0, 1,..., 6). According to the Judd-Ofelt theory, the $^5D_0$ - $^7F_{0,2,3,4,5,6}$ transitions are caused by the electric dipole, in which the PL intensity of the $^5D_0 - {}^7F_2$ transition is very sensitive to the Eu^{3+} ion surrounding environment. The $^5D_0 - {}^7F_1$ transition is due to the magnetic dipole and does not depend on the surrounding environment, so it is considered an internal standard to compare with the remaining transitions [12]. If the Eu^{3+} ions are occupied at the S_6 sites, the emission intensity of the $^5D_0 - {}^7F_2$ transition is weaker than that of the $^5D_0 - {}^7F_1$ transition. If the Eu^{3+} ions are occupied at the C_2 sites, the emission intensity of the $^5D_0 - {}^7F_2$ transition is stronger than that of the $^5D_0 - {}^7F_1$ transition [12]. The shape characteristic of the PL spectrum is related to the symmetry degree of the Eu^{3+} ion surrounding environment, and it can be recognized via the calculated value of the R_{21} ratio [1]. The R_{21} is equal to 1, indicating a symmetrical environment with the centrosymmetric S_6 site [13]. The R_{21} is greater than 1, indicating an asymmetrical environment with the non-centrosymmetric C_2 site [14].

The study wants to synthesize $Al_2O_3:Eu^{3+}$ NPs by a simple coprecipitation method. The strong PL ability of prepared $Al_2O_3:Eu^{3+}$ NPs at 614 nm will be suited for applications in optoelectronic and biomedicine.

2. Experiment

Chemicals were purchased from Sigma-Aldrich Eu_2O_3 (99.999%), $(NH_2)_2CO$ (purity ≥ 98%), $Al(NO_3)_3.9H_2O$ (99.99%), and NaOH (98%). The synthesis process of $Al_2O_3:Eu^{3+}$ (1 mol %) nanoparticles is carried out as follows: 0.018g of Eu_2O_3 was dissolved in 0.17 ml of HNO_3 solution to obtain an $Eu(NO_3)_3$ solution (A). 0.789 g $(NH_2)_2CO$, 3.712g $Al(NO_3)_3.9H_2O$, and 0.8g NaOH were sequentially dissolved in twice distilled water to get B, C, and D solutions, respectively. B, C, and D were added in the A to obtain a solution (F). The F was stirred at 100 ^{0}C for 1h and then kept overnight. The precipitate was filtered, washed several times, and dried at 80 ^{0}C for 15h. The obtained powder was calcined at 400 ^{0}C for 2h. Here, it is noted that in the case of Al_2O_3 synthesis, the $Eu(NO_3)_3$ solution was not used. The experimental steps are illustrated in **Figure 1**.

X-ray diffraction (XRD) patterns were recorded on a PANalytical Empyrean device with the Cu_K_α radiation (λ = 1.54056 Å, $2\theta = 15^o$ □ 70^o). Transmission electron microscopy (TEM), high-resolution transmission electron microscopy (HR-TEM), and selection area electron diffraction (SAED) images were performed on a JEOL - JEM 2100 device. The absorption spectra of the ultraviolet-visible (UV-Vis) region were recorded on the UV-2450 system. The photoluminescence (PL) spectra were recorded on a Spectra Pro2500i spectrophotometer under the 325 nm radiation of the He-Cd laser.

3. Result and Discussion

The crystal structure phase of Al_2O_3 and $Al_2O_3:Eu^{3+}$ NPs is studied via the XRD pattern in **Figure 2**. For Al_2O_3 NPs (**Figure 2a**), three peaks of 25.71, 45.85, and 66.66^0 correspond to the planes of α-

(012), γ-(400), and γ-(440), showing a structural phase mixing of hexagonal α-Al_2O_3 and cubic γ-Al_2O_3 structures (PDF data N°: 96-901-3047). For Al_2O_3:Eu^{3+} NPs, the XRD pattern still includes similar peaks. The structural parameters of the (012) planes were determined using a single peak fit tool of Origin software. The calculated values of 2θ angle and full width at half maximum (FWHM) are summarized as the insets in **Figure 2b**. The result shows that the FWHMs equal 0.194 and 0.177, meaning that the average crystal size of Al_2O_3 NPs can be smaller than that of Al_2O_3:Eu^{3+} NPs. The peak position of the (012) plane on the fitted line (solid line) for Al_2O_3 NPs is shifted towards the smaller 2θ angle of 25.38^0 for Al_2O_3:Eu^{3+} NPs. The peak-position shift depends on the annealing temperature and dopant ion concentration [15]. The nature of the peak shift is due to the difference between the dopant ion radius and the host ion radius, leading to the deformation of the host crystal lattice [16].

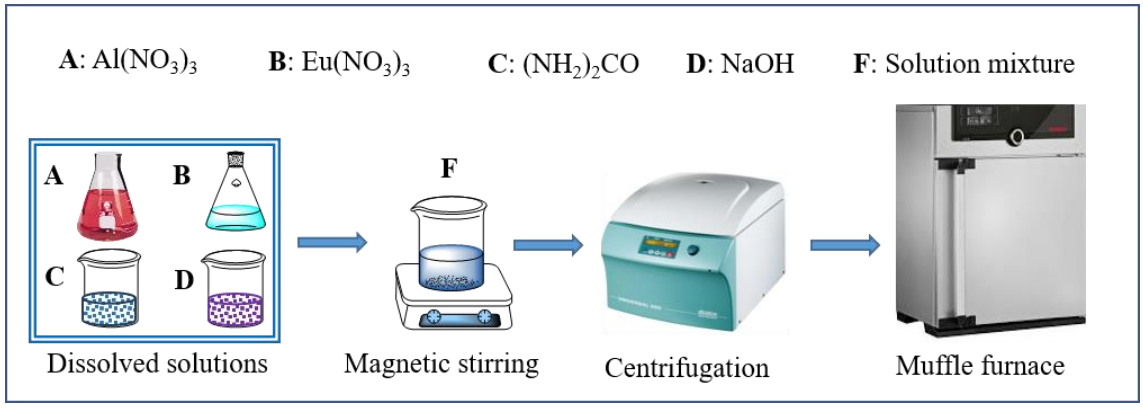

Figure 1. Schematic synthesis of Al_2O_3 and Al_2O_3:Eu^{3+} NPs

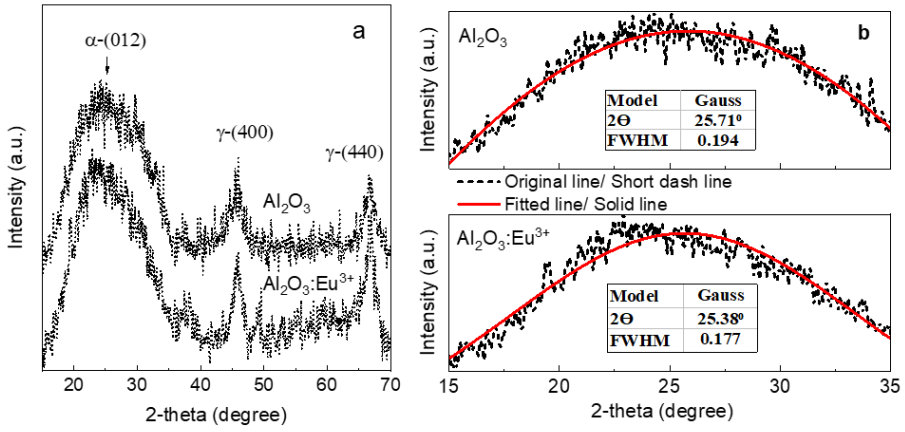

Figure 2. XRD pattern of Al_2O_3 and Al_2O_3:Eu^{3+} NPs (a) and the structural parameters of (012) planes (b)

The appearance of diffraction peaks shows that the quality of synthesized samples is better than that of samples prepared by the other method at 1 mol% Eu^{3+} concentration and 400 ^{0}C annealing temperature [8]. The observed characteristics from the XRD pattern are consistent with the observation of the Al_2O_3:Eu^{3+} (1 mol %) sample [1]. Hence, it can be considered that Eu^{3+} ions have been replaced in the Al_2O_3 crystal lattice.

Figure 3 shows the morphology of Al_2O_3 and Al_2O_3:Eu^{3+} NPs. Al_2O_3 NPs are agglomerated into large clusters with

crystal particle sizes of 12 - 15 nm (**Figure 3**). The HR-TEM image shows some areas with regular fringes, proving the crystalline structure, but there are also amorphous areas or imperfect crystals (**Figure 3b**) [17]. The SAED image consists of concentric bright circles representing the electron diffraction on the Al_2O_3 crystal planes (**Figure 3c**). These bright circles are consistent with the appearance of (012), (400), and (440) planes in the XRD pattern. A blurry bright circle corresponds to the broadband of the (012) plane, showing that the crystal is imperfect. When there is a replacement of Eu^{3+} ions in the Al_2O_3 lattice, the morphological and structural characteristics of Al_2O_3:Eu^{3+} NPs are almost unchanged (**Figure 3d, 3e,** and **3f**), as discussed for Al_2O_3 NPs.

Figure 4 presents the UV-Vis absorption spectra of Al_2O_3 and Al_2O_3:Eu^{3+} NPs. The absorption-peak position is located at 202 nm, characterizing to $2p(O^{2-}) \rightarrow 4f(Eu^{3+})$ transitions (**Figure 4a**). According to Taurc'formula, the E_g is expressed as [15]:

$$(\alpha h\nu) = A(h\nu - E_g)^n$$

where α is the absorption coefficient, A is the constant, h is Planck's constant, E_g is the band gap energy, ν is the absorption frequency, and n = 1/2 corresponds to the allowed direct transition [6]. Therefore, the E_g of Al_2O_3 NPs is calculated to be 5.26 eV, as shown in the inset in **Figure 4a**.

In the case of Al_2O_3:Eu^{3+} NPs, the absorption-peak position is shifted towards the larger wavelength of 220 nm (**Figure 4b),** so the E_g is also decreased to 4.72 eV (the inset of **Figure 4b)**. The E_g values are consistent with the results for doped Al_2O_3 NPs of α, and γ structure phase. The absorption-peak shift and the Eg decrease were also shown in Al_2O_3:Eu^{3+} ceramics [6] or the other doped semiconductors [18].

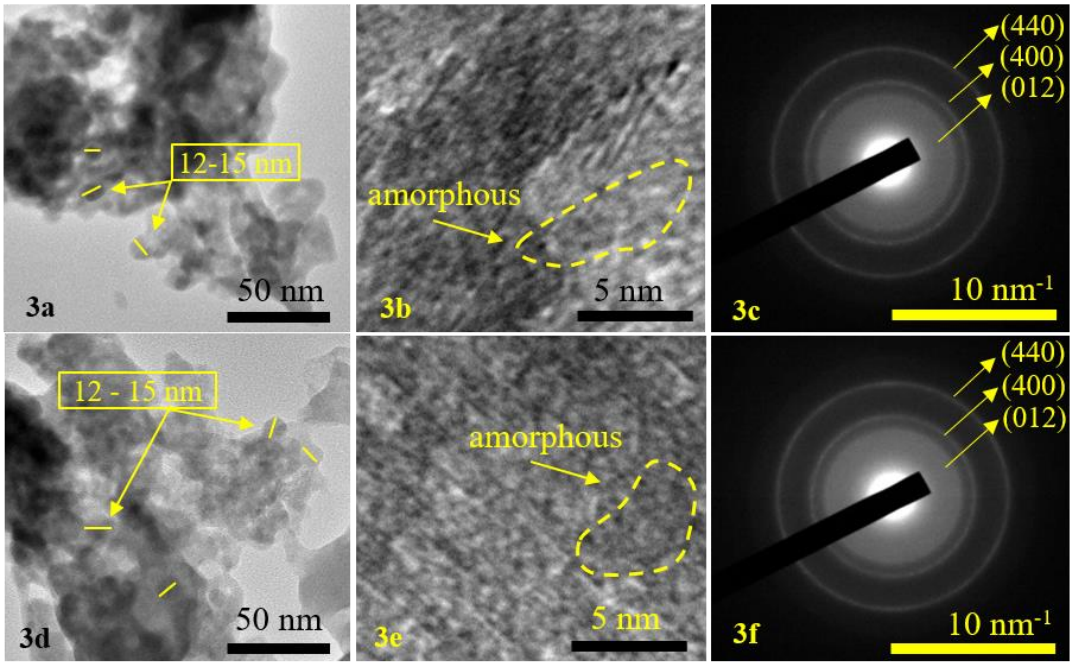

Figure 3. TEM, HRTEM, and SAED images of Al_2O_3 (3a, 3b, and 3c) and Al_2O_3:Eu^{3+} (3d, 3e, and 3f) NPs.

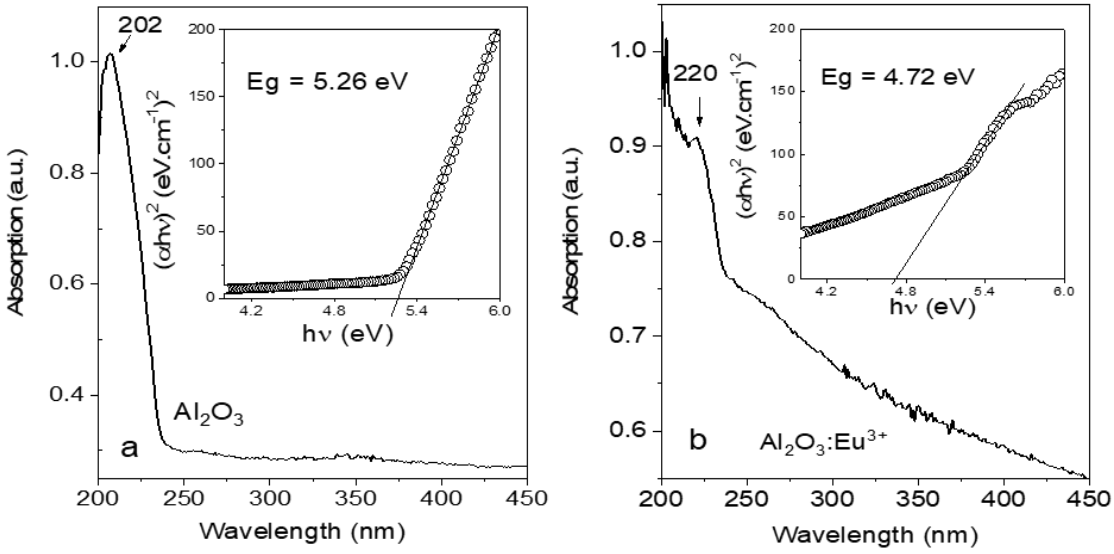

Figure 4. UV-Vis absorption spectra of Al_2O_3 NPs (a) and Al_2O_3:Eu^{3+} NPs (b)

Figure 5 presents the spectral properties of Al_2O_3 NPs and Al_2O_3:Eu^{3+} NPs. The PL spectrum of Al_2O_3 NPs shows an emission band with a 425 nm peak originating from defects [6], as inserted in **Figure 5a**. When the Eu^{3+} ions substitute in the crystal lattice, the PL spectrum of Al_2O_3:Eu^{3+} NPs is utterly superior to that of Al_2O_3 NPs (**Figure 5a**). However, the PL spectrum of Al_2O_3:Eu^{3+} NPs still has a 425 nm band with weak intensity, possibly due to the presence of defects of Al^{3+} ions or the transition $4f^65d^1 \rightarrow 4f^7(^8S^{7/2})$, belonging to Eu^{2+} ions on the surface of Al_2O_3:Eu^{3+} NPs [5].

The main PL band has a strong intensity representing transitions ($^5D_0 - {}^7F_J$) (J = 0, 1, 2, 3 due to the limit of the spectroscopy system) in the 4f electron shell of Eu^{3+} ions. The pre-eminent PL intensity of the $^5D_0 - {}^7F_J$ transition band compared with the PL intensity of the 425 nm band has been observed previously [11]. The $^5D_0 - {}^7F_J$ transitions are caused by electric and magnetic dipoles corresponding to the 578 nm ($^5D_0 - {}^7F_0$), 614 nm ($^5D_0 - {}^7F_2$), and 653 nm ($^5D_0 - {}^7F_3$), and 592 nm ($^5D_0 - {}^7F_1$) [1]. The ($^5D_0 - {}^7F_0$) and ($^5D_0 - {}^7F_3$) transitions are forbidden but are still observed due to J-mixing or wave function mixing of the $4f^6$ electron configuration. The $^5D_0 - {}^7F_1$ transition is not dependent on the Eu^{3+} ion surrounding environment, whereas the $^5D_0 - {}^7F_2$ transition is very sensitive [12]. The R_{21} between the emission line intensity I_{02} of the ($^5D_0 - {}^7F_2$) transition and the emission line intensity I_{01} of the ($^5D_0 - {}^7F_1$) transition is $R_{21} = \frac{I_{02}(^5D_0 \rightarrow {}^7F_2)}{I_{01}(^5D_0 \rightarrow {}^7F_1)}$ [13], in which I_{01} = 902364 (a.u.) and I_{02} = 2724817.5 (a.u) are calculated by integrating the emission bands, respectively. As a result, R_{21} = 3.02 > 1, so this value shows that the Eu^{3+} ion surrounding environment has a high asymmetry. The appearance of the PL band of ($^5D_0 - {}^7F_J$) transitions reaffirmed that Eu^{3+} ions have been replaced in the Al_2O_3 lattice. Even though Al_2O_3:Eu^{3+} NPs are only annealed at 400 ^{0}C for 2h, the 425 nm band has almost disappeared. This result of the coprecipitation method is similar to that of the sol-gel method [5]. The emission–absorption process in Al_2O_3:Eu^{3+} NPs is illustrated in **Figure 5b**.

4. Conclusion

Al_2O_3:Eu^{3+} NPs were successfully synthesized by the coprecipitation method. The α and γ mixed structural phase is formed at 400 ^{0}C annealing temperature. The crystal particle size is about 12 - 15 nm. The E_g of Al_2O_3 is decreased from 5.26 to 4.72 eV after doping with 1 mol % Eu^{3+} ion. The Al_2O_3:Eu^{3+} NPs have a strong PL intensity with an emission maximum of 614 nm, characterizing the $^5D_0 \rightarrow {}^7F_2$ transition of Eu^{3+} ions in Al_2O_3 crystal.

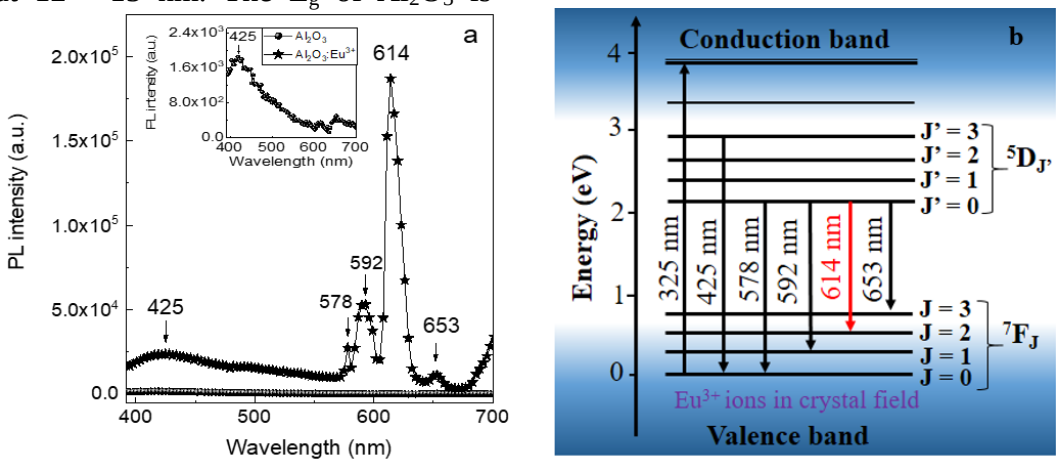

Figure 5. PL spectra of Al_2O_3 and Al_2O_3:Eu^{3+} NPs (a) and the energy diagram of the emission-absorption process (b)

5. Acknowledgment

This paper has been funded by the NAFOSTED project (Number code: 103.03-2020.08) due to the support of the Vietnam National Foundation for Science and Technology Development.

6. References

[1] Daiane H.S. Reis, Juliana M.M. Buarque, Marco A. Schiavon, Edison Pecoraro, Sidney José L. Ribeiro, Jefferson L. Ferrari, (2015). Simple and cost-effective method to obtain RE^{3+}-doped Al_2O_3 for possible photonic applications. *Ceramics International*, **41**, 10406–10414.

[2] Amrita Das, Vishal Shama, (2016). Synthesis And Characterization Of Eu^{3+} Doped α-Al_2O_3 Nanocrystalline Powder For Novel Application In Latent Fingerprint Development. *Advanced Materials Letters*, **7(4)**, 302-306.

[3] R. Klement, K. Drdlíkova´, M. Kachlík, D. Drdlík, D. Galusek, K. Maca, (2021). Photoluminescence and optical properties of Eu^{3+}/Eu^{2+}-doped transparent Al_2O_3 ceramics. *Journal of the European Ceramic Society*, **41(9)**, 4896 - 4906.

[4] Min Zhang, Yibo Wu, Lin Zhang, Haoran Zhang, Boyang Cui & Zongxu Sun, (2017). Photoluminescence properties of Eu^{3+}-doped stalk-like Al_2O_3 via a hydrothermal route followed by heat treatment. *Advances in Applied Ceramics*, **117(5),** ISSN: 1743-6753 (Print) 1743-6761.

[5] J. Wrzyszcz, W. Mista, D. Hreniak, W. Strek, M. Zawadzki, H. Grabowska, (2002). Preparation and optical properties of nanostructured europium-doped. *Journal of Alloys and Compounds*, **341(1-2)**, 358–361.

[6] Nikifor Rakov, Francisco E. Ramos, Gustavo Hirata, and Mufei Xiao, (2003). Strong photoluminescence and cathodoluminescence due to f – f transitions in Eu^{3+}-doped Al_2O_3 powders prepared by direct combustion synthesis and thin films deposited by laser ablation. *Applied Physics Letters*, **83(2)**, 272-274.

[7] R. Bharthasaradhi & L.C. Nehru, (2016). Structural and phase transition of α- Al_2O_3

powders obtained by coprecipitation method. *Phase Transitions*, **89(1)**, 77-83.

[8] M.A.F. Monteiro, H.F. Brito, M.C.F.C.M. Felinto, G.E.S. Brito, E.E.S. Teotonio, F.M. Vichi, R. Stefani, (2008). Photoluminescence behavior of Eu^{3+} ion doped into c- and a-alumina systems prepared by combustion, ceramic, and Pechini methods. *Microporous and Mesoporous Materials*, **108(1-3)**, 237–246.

[9] S.Toyoda, T. Shinohara, H. Kumigashira, M. Oshima, and Y. Kato, (2012). Significant increase in conduction band discontinuity due to solid phase epitaxy of Al_2O_3 gate insulator films on GaN semiconductor. *Applied Physics Letters*. **101(23)**, 231607.

[10] Elena O. Filatova and Aleksei S. Konashuk, (2015). Interpretation of the Changing the Band Gap of Al_2O_3 Depending on Its Crystalline Form: Connection with Different Local Symmetries. *The Journal of Physical Chemistry C*, **119(35)**, 20755-20761.

[11] E.F. Huerta, I. Padilla, R. Martinez-Martinez, J.L. Hernandez-Pozos, U. Caldiño, C. Falcony, (2012). Extended decay times for the photoluminescence of Eu^{3+} ions in aluminum oxide films through interaction with localized states. *Optical Materials*, **34(7)**, 1137–1142.

[12] K. Binnemans, (2015). Interpretation of europium (III) spectra. *Coordination Chemistry Reviews*, **295**, 1-45.

[13] Dianguang Liu, and Zhenfeng Zhu, (2014). Photoluminescence properties of the Eu-doped alpha- Al_2O_3 microspheres. *Journal of Alloys and Compounds*, **583**, 291–294.

[14] Nikifor Rakov, Glauco S. Maciel, Whualkuer Lozano B., and Cid B. de Araújo, (2007). Europium luminescence enhancement in Al_2O_3:Eu^{3+} powders prepared by direct combustion synthesis. *Journal of Applied Physics*, **101(3)**, 036102-036102-3.

[15] Chuc Ngoc Pham, Quyen Van Trinh, Dang Van Thai, Nhiem Ngoc Dao, Bac Quang Nguyen, Dung Trung Doan, Hung Bao Le, Vinh Van Nguyen, Lim Thi Duong, Lam Dai Tran, (2022). Synthesis of CeO_2-Fe_2O_3 Mixed Oxides for Low-Temperature Carbon Monoxide Oxidation. *Adsorption Science & Technology*, Article ID 5945169, 12 pages.

[16] Sandeep Kumar, Ram Prakash, Vinay Kumar, G.M. Bhalerao, R.J. Choudhary, D.M., (2015). Surface and spectral studies of Eu^{3+}-doped α-Al_2O_3 synthesized via solution combustion synthesis. *Advanced Powder Technology*, **26(4),** 1263-1268.

[17] Wei-Ning Wang, W. Widiyastuti, Takashi Ogi, I. Wuled Lenggoro, and Kikuo Okuyama, (2007). Correlations between Crystallite/Particle Size and Photoluminescence Properties of Submicrometer Phosphors. *Chemistry of Materials*, **19(7)**, 1723-1730.

[18] Hong Van Bui, Dang Van Thai, Tien Dai Nguyen, Van Nang Lam, Huu Toan Tran, Van Manh Nguyen, Nguyen Duc Nui, Nguyen Manh Hung, (2023). Mn-doped ZnS nanoparticle photoanodes: Synthesis, structural, optical, and photoelectrochemical characteristics. *Materials Chemistry and Physics*, **307**, 128081.